Original Article

ANKRD11 as a potential biomarker for brain metastasis from lung adenocarcinoma via cerebrospinal fluid liquid biopsy

Qinhong Sun[1#^], Peng Xing[1,2#], Qinglin Wang[1#], Zhijun Xia[1], Jianyu Li[1], Zhitong Li[1], Fancheng Meng[1], Tongyan Liu[1], Siwei Wang[1^], Rong Yin[1,3,4^]

[1]Department of Thoracic Surgery, Jiangsu Key Laboratory of Molecular and Translational Cancer Research, Nanjing Medical University Affiliated Cancer Hospital & Jiangsu Cancer Hospital & Jiangsu Institute of Cancer Research, Nanjing, China; [2]Department of Oncology, Jing County Hospital, Xuancheng, China; [3]Biobank of Lung Cancer, Jiangsu Biobank of Clinical Resources, Nanjing, China; [4]Collaborative Innovation Center for Cancer Personalized Medicine, Nanjing Medical University, Nanjing, China

Contributions: (I) Conception and design: Q Sun, P Xing; (II) Administrative support: S Wang, R Yin; (III) Provision of study materials or patients: P Xing; (IV) Collection and assembly of data: Q Sun; (V) Data analysis and interpretation: Q Sun; (VI) Manuscript writing: All authors; (VII) Final approval of manuscript: All authors.

[#]These authors contributed equally to this work.

Correspondence to: Rong Yin, MD, PhD. Department of Thoracic Surgery, Jiangsu Key Laboratory of Molecular and Translational Cancer Research, Nanjing Medical University Affiliated Cancer Hospital & Jiangsu Cancer Hospital & Jiangsu Institute of Cancer Research, Baiziting 42, Nanjing 210009, China; Biobank of Lung Cancer, Jiangsu Biobank of Clinical Resources, Nanjing, China; Collaborative Innovation Center for Cancer Personalized Medicine, Nanjing Medical University, Nanjing, China. Email: rong_yin@njmu.edu.cn; Siwei Wang, MD, PhD. Department of Thoracic Surgery, Jiangsu Key Laboratory of Molecular and Translational Cancer Research, Nanjing Medical University Affiliated Cancer Hospital & Jiangsu Cancer Hospital & Jiangsu Institute of Cancer Research, Baiziting 42, Nanjing 210009, China. Email: wangsiwei@njmu.edu.cn.

Background: Brain metastasis (BM) explains the majority of lung cancer-related mortality, especially lung adenocarcinoma (LUAD). The extensive clinical adoption of liquid biopsy presents a minimally invasive approach for the early detection and treatment management of brain metastasis from lung adenocarcinoma (BM-LUAD). Nonetheless, biomarkers for assessing BM-LUAD remain insufficient. This study aims to reveal novel biomarkers for BM-LUAD through the liquid biopsy of cerebrospinal fluid (CSF).

Methods: Circulating tumor DNA (ctDNA)-based panel sequencing was conducted on CSF samples from seven patients with BM-LUAD. Additionally, single-cell RNA sequencing (scRNA-seq) data from normal lung tissue, primary tumors, and BMs were analyzed using publicly available datasets. Functional assays were performed on cell lines, complemented by *in vivo* studies in nude mice.

Results: CSF liquid biopsy identified high-frequency mutations in *EGFR*, *BRCA2*, and *ANKRD11* among patients with BM-LUAD. Further analysis highlighted *ANKRD11* as a potential biomarker, showing reduced expression in tumor tissues and significant prognostic implications. ScRNA-seq revealed a progressive decrease in *ANKRD11* expression along tumor progression, while *in vitro* and *in vivo* assays confirmed its role in suppressing tumor invasion and metastasis.

Conclusions: Our study highlights the potential of ctDNA-based CSF liquid biopsy in identifying BM-LUAD, and the efficacy in revealing novel biomarkers for BM-LUAD. Data analyses and functional assays indicated *ANKRD11* as a predictive biomarker for BM-LUAD. This result addresses, to some extent, the existing gap in biomarkers for BM-LUAD.

Keywords: Lung adenocarcinoma (LUAD); brain metastasis (BM); liquid biopsy; cerebrospinal fluid (CSF); biomarker

^ ORCID: Qinhong Sun, 0009-0007-1321-201X; Siwei Wang, 0000-0001-5077-060X; Rong Yin, 0000-0002-9744-4251.

Submitted Sep 06, 2024. Accepted for publication Jan 15, 2025. Published online Mar 03, 2025.
doi: 10.21037/tlcr-24-800
View this article at: https://dx.doi.org/10.21037/tlcr-24-800

Introduction

The prognosis of advanced-stage lung adenocarcinoma (LUAD) remains poor, with a 5-year survival rate of less than 20%, primarily due to its tendency to metastasize to distant organs, especially brain (1,2). Brain metastasis from lung adenocarcinoma (BM-LUAD) occurring in approximately 20–40% of patients, which contributes significantly to the morbidity and mortality of LUAD (3,4). The complex and multifaceted nature of BM underscores the urgent need to understand the molecular mechanisms driving this process to develop effective therapeutic strategies.

Traditional tissue biopsies, while providing valuable information, pose significant challenges in the context of BMs. The invasive nature of the procedure, coupled with the delicate and critical location of brain lesions, limits the feasibility and safety of obtaining tissue samples. This has spurred interest in non-invasive techniques such as liquid biopsy. Liquid biopsy involves the analysis of circulating tumor DNA (ctDNA), circulating tumor cells and other biomarkers in bodily fluids like blood and cerebrospinal fluid (CSF) (5). CSF, in particular, offers a unique and promising source for detecting genetic alterations associated with BMs due to its proximity to the central nervous system (6).

The application of liquid biopsy in the management of lung cancer has shown great promise, providing real-time insights into tumor dynamics and genetic alterations without the need for invasive procedures. However, despite its potential, the current landscape of biomarkers for BM remains sparse (7,8). The identification of reliable biomarkers is crucial for early detection, monitoring treatment response, and guiding therapeutic decisions (9). The lack of specific and sensitive biomarkers for BM-LUAD hampers the ability to effectively diagnosis and treatment.

In this study, we aimed to identify novel biomarkers for BM-LUAD using ctDNA-based liquid biopsy. By leveraging the advantages of CSF liquid biopsy and ctDNA sequencing, we sought to uncover genetic alterations that could serve as potential biomarkers. Our results demonstrated that *ANKRD11* emerged as a frequently mutated gene in CSF from patients with BM-LUAD. The *ANKRD11* alteration, particularly loss-of-function mutations, emphasizes its potential involvement in the metastatic process and highlights its importance as a biomarker for BM. We present this article in accordance with the ARRIVE and MDAR reporting checklists (available at https://tlcr.amegroups.com/article/view/10.21037/tlcr-24-800/rc).

Highlight box

Key findings

- Using circulating tumor DNA (ctDNA)-based cerebrospinal fluid (CSF) liquid biopsy, *ANKRD11* mutation was revealed to be associated with brain metastasis from lung adenocarcinoma (BM-LUAD).
- Single-cell RNA sequencing analyses, *in vitro* and *in vivo* assays indicated *ANKRD11* as a predictive biomarker for BM-LUAD.

What is known and what is new?

- CSF liquid biopsy enables a relatively non-invasive assessment of the mutational features in patients with BM-LUAD, aiding in the monitoring of metastasis risk and treatment management.
- This study identifies a novel biomarker for BM-LUAD through ctDNA-based CSF liquid biopsy, further demonstrating its clinical applicability and advantages.

What is the implication, and what should change now?

- This finding suggests that CSF liquid biopsy could become a pivotal tool in early detection and monitoring of BM-LUAD, potentially enabling more timely and personalized treatment interventions.
- CSF liquid biopsy could be recommended as an important procedure for patients with suspected or confirmed BM-LUAD. Further research could validate these findings in larger cohorts and explore combining CSF liquid biopsy with other diagnostic methods to enhance detection accuracy and reliability, ultimately improving patient outcomes through earlier intervention and more effective management of metastatic lung cancer.

Methods

Sample collection and data processing

CSF samples were collected from seven patients with BM-LUAD, detailed inclusion and exclusion criteria for the patients are provided in the Table S1. Clinical and pathological characteristics of the seven patients are summarized in Table S2, including age, gender, smoking history, stage, pathological subtypes, treatment types,

BM site, size of BMs, *EGFR* mutation status, *ANKRD11* mutation status, and disease progression. The collection was performed under sterile conditions using lumbar puncture. Approximately 5–10 mL of CSF was obtained from each patient and immediately processed to ensure sample integrity. The study was conducted in accordance with the Declaration of Helsinki (as revised in 2013) and was approved by the Ethics Committee of the Jing County Hospital (No. 2020-007). Written informed consent was obtained from all patients included in the study.

The collected CSF samples underwent panel sequencing to identify potential genetic mutations associated with BMs. Quality control of DNA samples was performed using three main methods: agarose gel electrophoresis to analyze DNA degradation and RNA contamination, Nanodrop to measure DNA purity ($OD_{260/280}$ ratio), and Qubit for precise quantification of DNA concentration. DNA samples with an OD value between 1.8 and 2.0 and a concentration above 100 ng were used for library construction. For tumor tissue, genomic DNA was extracted from paraffin-embedded samples using the HiPure FFPE DNA Kit (D3126-03, Magen, Guangzhou, China), and fragmented into 150–230 bp pieces using a sonicator. Libraries were prepared and hybridized using the SureSelectXT Reagent kit (G9611A, Agilent, Santa Clara, CA, USA) and custom probes. Similarly, genomic DNA from leukocytes was extracted using the HiPure Blood DNA Mini Kit (D3111-03, Magen), fragmented, and processed as described above. Cell-free DNA was extracted from blood using the HiPure Circulating DNA Midi Kit A, and libraries were constructed using the KAPA HyperPrep Kit (KK8504, Roche, Wilmington, Massachusetts, USA). Custom probes and the SureSelectXT Reagent kit (G9611A, Agilent) were used for capture. Following PCR amplification, libraries were quality controlled. Initial quantification was performed using Qubit 2.0, followed by Agilent 2100 to check insert size. If the insert size met expectations, the effective concentration was accurately quantified using qPCR to ensure a concentration of 3 nmol/L. Libraries passing quality control were sequenced using the Illumina Novaseq PE150 platform, which involves high-throughput paired-end sequencing with each end sequenced to 150 bp.

Mutation calling

In this study, targeted panel sequencing was performed to identify mutations within a predefined set of genes. Raw sequencing reads were aligned to the hg19 reference genome using BWA, followed by PCR duplicate removal and base quality score recalibration using GATK. Variant calling was conducted using GATK's HaplotypeCaller, which detects single nucleotide variants (SNVs) and insertions-deletions (Indels) within the targeted regions. Variants were filtered based on quality metrics (e.g., quality score >30, depth >100×) and functionally annotated using ANNOVAR or SnpEff. Common variants (MAF >1%) and known artifacts were excluded to enhance specificity. Selected variants were validated through orthogonal methods such as Sanger sequencing to confirm accuracy.

Re-analyses of publicly available datasets

The single-cell RNA expression profiles of 11 primary tumors and 10 BMs, sourced from GSE131907 by Kim *et al.* (10), were sequenced using the Illumina HiSeq 2500 platform. These 21 samples from patients with BM-LUAD were obtained through surgical resection, with no prior treatment administered. The Cancer Genome Atlas (TCGA) LUAD cohort provided bulk RNA-seq data, including raw counts and fragments per kilobase per million normalized values, along with comprehensive clinicopathological and follow-up information for 499 patients, accessed via the TCGA database (https://portal.gdc.cancer.gov/). Additionally, reverse phase protein array-based proteomics data for 345 LUAD patients were retrieved.

InferCNV analysis

InferCNV (v1.6.0) was used to detect copy number variations (CNVs) in single-cell RNA sequencing (scRNA-seq) data. Data were preprocessed and normalized using R (v4.2.1). Cells were grouped into reference (normal) and observation (primary tumors and BMs) sets. The inferCNV algorithm applied smoothing and identified CNVs through deviations in gene expression, visualized with heatmaps. Validation compared inferred CNVs to known regions, revealing genetic alterations in various cellular states and diseases (11).

Library preparation and sequencing depth of the public scRNA-seq data

Each cell suspension was subjected to 3' scRNA-seq using Single Cell A Chip Kit, Single Cell 3' Library and Gel Bead Kit V2, and i7 Multiplex Kit (10× Genomics,

Pleasanton, CA, USA) with a cell recovery target of 5,000, following the manufacturer's instructions. Libraries were sequenced on an Illumina HiSeq2500, and mapped to the GRCh38 human reference genome using the Cell Ranger toolkit (version 2.1.0).

Processing of scRNA-seq data and cell type annotations

Seurat (v4.0) was applied for data processing and visualization (12). After examining the overall cellular landscape, a total of 9,860 epithelial cells were extracted from normal lung, primary tumors, and BMs for further analysis. Using highly variable genes, principal component analysis was conducted to identify significant dimensions, termed principal components. Subsequently, clustering analysis was performed, followed by cell annotation based on the distinctive gene expression profiles of each cluster.

Pseudo-time trajectory construction

To investigate the progression trajectory of LUAD cell, we used minimal spanning tree algorithm-based monocle (v2.0) R-package to perform a pseudo-time analysis (13).

Differentially expressed genes (DEGs)

DEGs were identified by calculating fold-change and P value between "treatment" and control groups. We set a twofold cutoff of fold change and false discovery rate adjusted P<0.01 as the criteria for DEG selection. This was done by using the limma package of R project.

Transwell assay

Cells were seed at upper microholed wells with the Matrigel plate. The wells were placed into the lower well containing 500 µL of complete medium. 37 ℃, 12 h, cells were gently removed in the upper wells with a cotton swab. The cells in the lower chamber were fixed for 10 min and stained with 1% crystal violet dye in 2% ethanol for 15 min.

Wound-healing assay

A pipette tip was used to scratch a line on the cell layer when the cells reached at 90% confluency. The picture of each wound was recorded by microscope after 0 and 24 h. ImageJ software (v1.50i) was used to calculate the mean value of the distance of each wound.

Nude mice tumor model construction and imaging observation of BM

Four-week-old female BALB/c nude mice were purchased from Gem Pharmatech (Nanjing, China). All animal experiments were conducted under a project license (No. IACUC2404078) approved by the Institutional Animal Care and Use Committee (IACUC) of Nanjing Medical University, in compliance with the national and institutional guidelines for the care and use of laboratory animals. To ensure the statistical power and reduce potential bias in the experimental results, at least 10 BALB/c nude mice were randomly assigned to each experimental group (*ANKRD11* knockdown group and control group). The sample size was determined based on a priori power analysis. Researchers conducting imaging and data analysis were blinded to the group allocations to minimize observer bias. Humane endpoints were established, including a weight loss of more than 20% and the appearance of significant neurological symptoms. Fluorescently labeled A549 cells (1×10^6 cells/100 µL) were injected into the left cardiac ventricle of anesthetized nude mice. Four weeks post-injection, *in vivo* fluorescence computerized tomography imaging was performed to evaluate the size and distribution of BMs. Quantitative analysis of fluorescence signals was conducted using image analysis software to assess the extent of BM. Mice were then sacrificed, and the brains were harvested, weighed, fixed, and sectioned for histological examination. Fluorescence microscopy was utilized to detect and quantify metastatic cells.

Hematoxylin and eosin (HE) staining of brain tissue in model mice

The brain tissues of model mice were obtained every 5 µm per step until HE staining revealed potential metastasis sites. The sections stained with hematoxylin solution for 5 min and put in 1% acid ethanol (1% HCl in 70% ethanol) and then rinsed in distilled water. Then stained with eosin solution for 2 min and followed by dehydration with graded alcohol and clearing in xylene.

Statistical analysis

Statistical analyses were performed using R (v4.2.1). For comparisons of the continuous variables between groups, Wilcoxon rank-sum tests were used. For comparisons of the categorical variables paired between groups, McNemar Chi-squared tests were used. All reported P values were two-sided. The differences were considered significant when

the P value was <0.05. Other figures were generated using the R package ggplot2. Kaplan-Meier survival analysis was conducted to evaluate the prognostic significance of gene expression in LUAD patients. The analysis was performed using the Kaplan-Meier Plotter online tool (https://kmplot.com/) (14,15).

Results

Mutational features of CSF from patients with BM-LUAD using ctDNA-based liquid biopsy

This study was conducted using CSF samples from seven patients with BM-LUAD, with the workflow illustrated in the diagram (*Figure 1A*). Our results indicated a high mutation frequency in several driver genes, including *EGFR*, *BRCA2*, and *ANKRD11*, which emerged in the most of CSF samples (four in seven). The classification of mutations included missense mutations, frame-shift deletions, in-frame deletions, frame-shift insertions, and multi-hit events (*Figure 1B*). The observed mutations included various types such as single nucleotide polymorphisms (SNP), insertions and deletions. Multi-hit events, which refer to multiple mutations occurring within the same gene, are difficult to detect due to its low concentration in ctDNA of body fluids (16). This highlights the robustness of our sequencing approach. As is shown in the upper section of the plot (*Figure 1C*), SNPs were the most common variant type, followed by insertions and deletions. Specific nucleotide changes, such as C>G and C>A, were prominently featured, which is more frequently observed in patient with a history of smoking or prolonged exposure to secondhand smoke (17), in accordance with patients' history in our study. Additionally, the lower section of the plot shows a median of 18 variants per sample, with the top 10 most frequently mutated genes listed. Furthermore, the distinction between transition (Ti) and transversion (Tv) mutations is depicted, with Tvs occurring more frequently than Tis (*Figure 1D*). A higher Ti/Tv ratio, particularly an increased frequency of Tvs, is often associated with higher genomic instability. Genomic instability is a hallmark of cancer that contributes to the aggressive behavior of tumors (18) such as metastasis, which is consistent with the patient condition in our study.

Identification of BM-related mutation and its prognostic impact on patients with LUAD

We further explored the frequently mutated signaling pathways enriched in the CSF samples from patients with BM-LUAD, including RTK-RAS, PI3K, TP53, WNT, TGF-beta, NOTCH, and cell-cycle-related genes. The RTK-RAS pathway exhibited the highest mutation frequency at 71.43%, followed by the PI3K pathway at 57.14%, and TP53 and WNT pathways each at 42.86% (*Figure 2A*). Then we performed co-occurrence and mutual exclusivity analyses of the most frequently mutated genes. Notably, *ANKRD11* mutations show significant co-occurrence with *EGFR* and *BRCA2* mutations (P<0.05) (*Figure 2B*). These results indicated that *ANKRD11* mutations were enriched in RTK-RAS activated or *EGFR*-mutated LUADs.

To further validate this observation, we analyzed publicly available cfDNA data from a cohort of non-brain metastatic NSCLC patients (Figure S1). Remarkably, *ANKRD11* mutations were not detected in any of the ctDNA samples from this cohort, resulting in a mutation rate of 0%. Besides, based on detailed patient data (see Table S2), *ANKRD11* mutations were associated with significantly larger brain metastatic lesions compared to cases without the mutation (Figure S2). Statistical analysis using the Mann-Whitney *U* test revealed a significant difference in lesion size between the two groups (P=0.049). This finding suggests that *ANKRD11* mutations may contribute to an increased metastatic potential in the brain. Therefore, we decided to investigate the association between this gene and clinical prognosis. We estimated the survival outcomes of LUAD patients with or without *ANKRD11* mutations. Kaplan-Meier survival analyses indicated a trend towards shorter overall survival (OS) in patients harboring *ANKRD11* mutations compared to those without, although this difference did not reach statistical significance (P=0.24) (*Figure 2C*). Additionally, we analyzed the expression level of *ANKRD11* in LUAD tissues using data from TCGA. Our analysis revealed that the expression level of *ANKRD11* was significantly lower in tumor tissues compared to normal tissues (P=0.04), suggesting a potential tumor suppressor role of *ANKRD11* (*Figure 2D*). Furthermore, survival analysis shown that patients with lower *ANKRD11* expression had poorer prognosis, highlighting its prognostic significance [logrank P<0.001] (*Figure 2E*). To further validate our findings, we analyzed two publicly available datasets to compare the prevalence of *ANKRD11* mutations in BMs and non-brain metastatic lung cancer (Figure S3). In the dataset of non-brain metastatic sites (Dataset 1) (19), only 1% of patients exhibited *ANKRD11* mutations, suggesting that such mutations are rare in non-brain metastatic settings. In contrast, the dataset of confirmed BMs (Dataset 2) (20) revealed that 7% of patients harbored

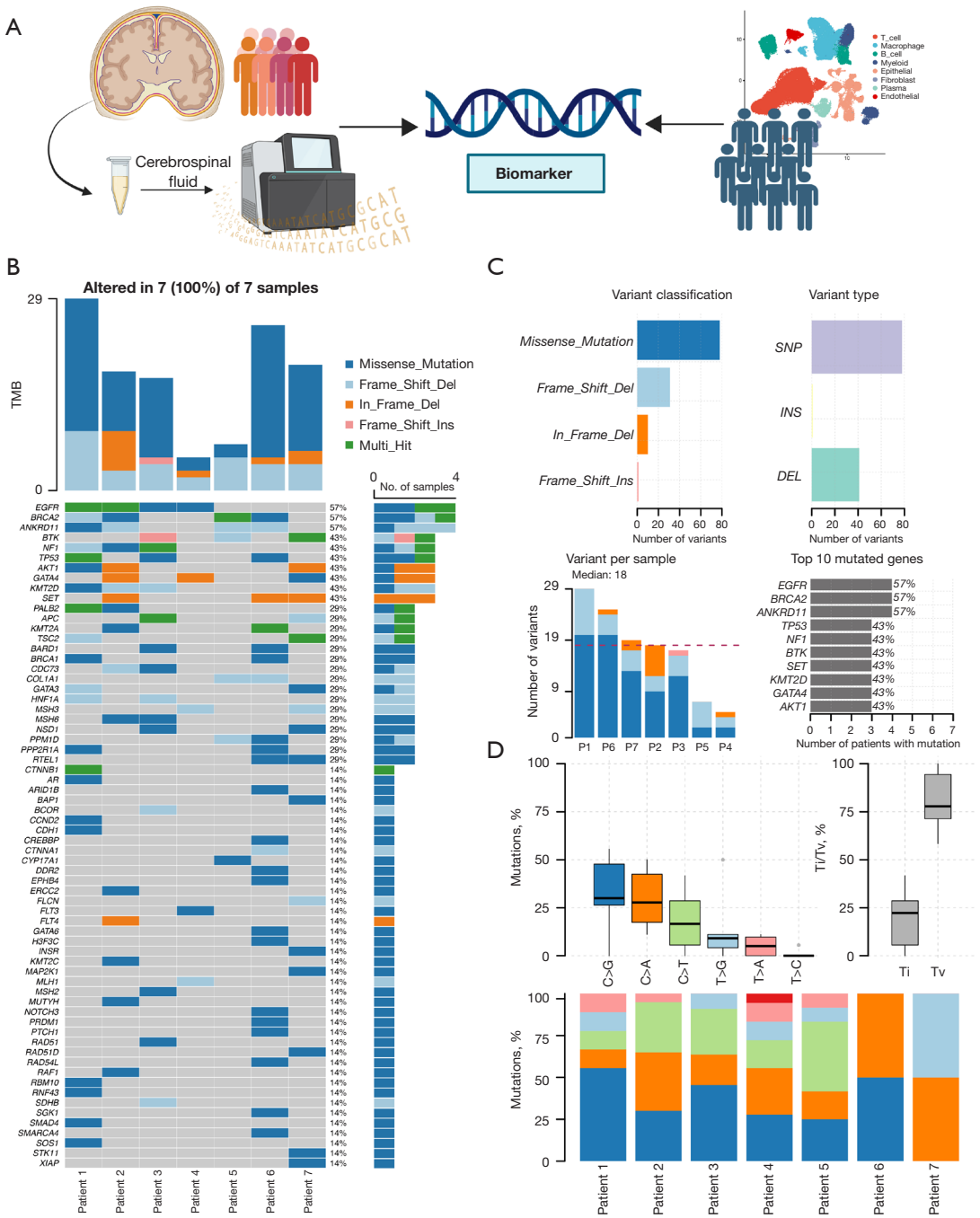

Figure 1 Mutational landscape of ctDNA in CSF from patients with BM-LUAD. (A) Panel sequencing of ctDNA in 7 CSF samples from 7 patients with BM-LUAD was performed to identify genetic alterations, and the data were subsequently analyzed, revealing a novel biomarker. The findings were further validated using public single-cell datasets and both *in vivo* and *in vitro* experiments. (B) Heatmap illustrating the mutational landscape across 7 CSF samples from patients with BM-LUAD. (C) The upper section presents summary of variants classification and types, the lower section shows the median number of variants per sample and lists the top 10 most frequently mutated genes. (D) Distribution and frequency of mutation types. The upper section shows the percentage of each mutation type and the Ti/Tv ratio across the samples. The lower section provides a breakdown of mutation types for each individual sample. SNP, single nucleotide polymorphism; INS, insertion; DEL, deletion; BM, brain metastasis; Ti, transition; Tv, transversion; ctDNA, circulating tumor DNA; CSF, cerebrospinal fluid; LUAD, lung adenocarcinoma; TMB, tumor mutation burden.

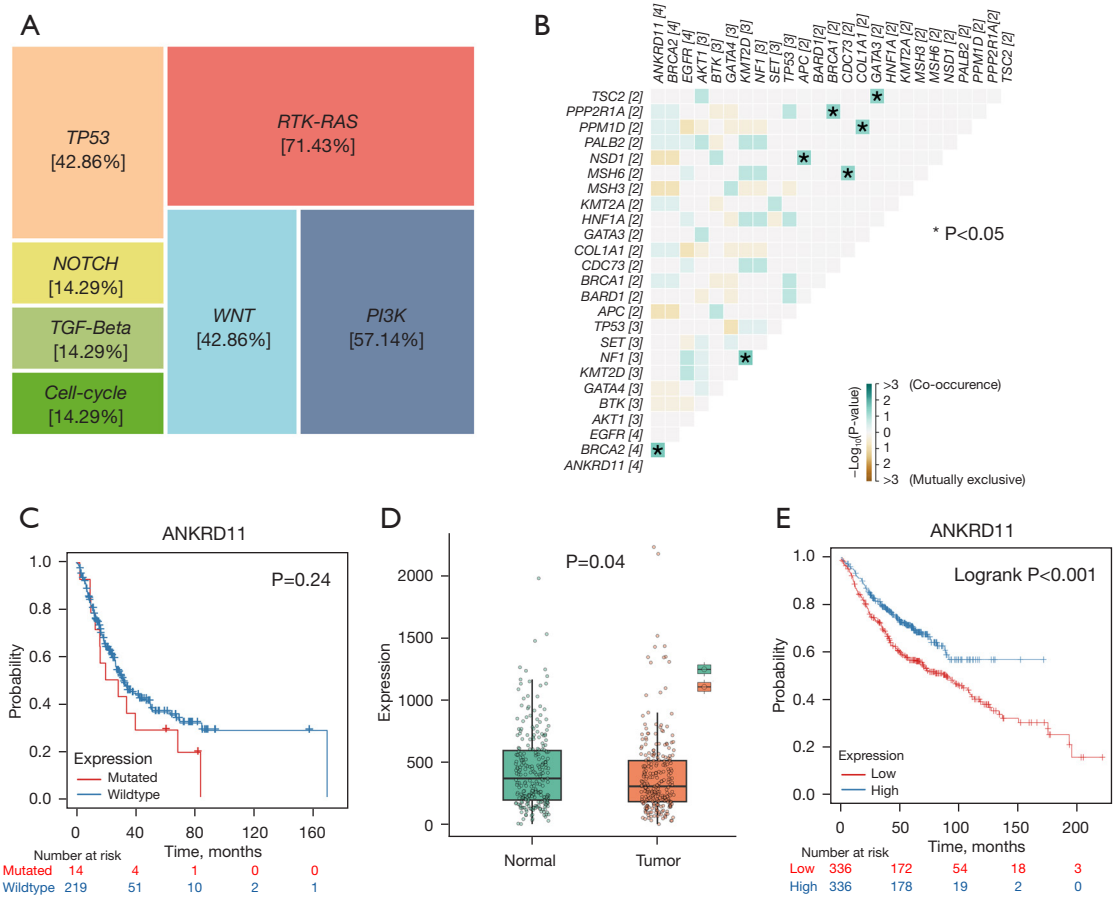

Figure 2 A potential biomarker was identified through concurrence landscape, differential expression and prognosis analysis. (A) Pathway analysis of the most frequently mutated genes identified in CSF samples. Key signaling pathways involved include RTK-RAS (71.43%), PI3K (57.14%), TP53 (42.86%), WNT (42.86%), NOTCH (14.29%), TGF-beta (14.29%), and cell-cycle (14.29%). (B) Co-occurrence and mutual exclusivity analysis of the top mutated genes. Significant co-occurrence (P<0.05) is marked with stars. (C) Kaplan-Meier survival analysis of LUAD patients based on *ANKRD11* mutation status. (D) Box plot comparing *ANKRD11* expression levels in normal lung tissues versus tumor tissues. *ANKRD11* expression was significantly lower in tumor tissues compared to normal tissues. (E) Kaplan-Meier survival analysis of LUAD patients based on *ANKRD11* expression levels. CSF, cerebrospinal fluid; LUAD, lung adenocarcinoma.

ANKRD11 mutations. Statistical analysis using the Chi-square test demonstrated a significant difference in mutation rates between the two datasets (P<0.001). These results highlight the specificity of *ANKRD11* mutations in BMs and further support its potential as a biomarker for BM-LUAD.

Single-cell analysis revealing expressional pattern of ANKRD11 as BM-LUAD biomarker

The enrichment of *ANKRD11* mutation in CSF of patients with BM-LUAD, combined with its differential expression and the association with prognosis, suggests that *ANKRD11* could serve as a potential biomarker for BM-LUAD. To further elucidate the role of *ANKRD11* in patients with BM-LUAD, we performed analyses on single-cell cell data from normal lung tissue, primary lung tumors, and BMs. Using data from a public database, we identified 28 distinct cell clusters, illustrating the cellular diversity within these samples (*Figure 3A*). Each cluster was further annotated to reveal a variety of cell types, including T cells, macrophages, B cells, myeloid cells, epithelial cells, fibroblasts, plasma cells, and endothelial cells (*Figure 3B*). This comprehensive cell type identification provides a detailed landscape of the cellular constituents in LUAD and its BMs.

Then, we focused on epithelial cells, extracting them

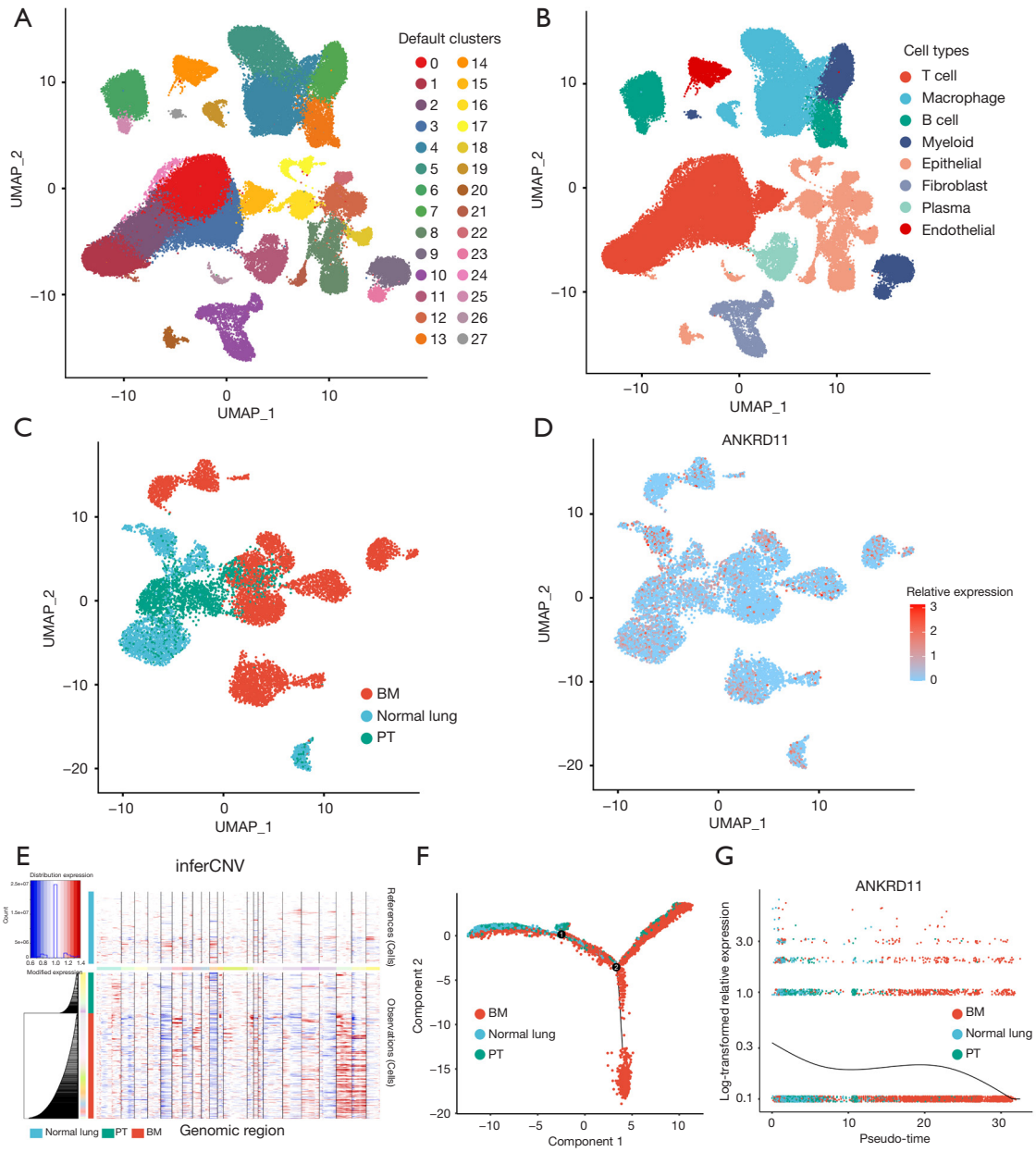

Figure 3 The expression trajectory of the target biomarker during lung cancer progression and metastasis was revealed through single-cell analysis. (A,B) The UMAP plot of cells including normal lung samples, primary lung tumor and brain metastasis samples was color-coded by clusters (A) and cell types (B). (C) The UMAP plot of epithelial cells extracted for further clustering analysis, with cells colored according to sample origin. (D) Different expression levels of *ANKRD11* across different tissue origins, with higher *ANKRD11* expression observed in normal lung tissue and primary lung tumors, and lower expression in brain metastasis samples. (E) Hierarchical heatmaps displaying large-scale CNVs of epithelial cells from normal lung, primary tumor, and brain metastasis samples. Gains or losses were inferred by averaging expression over 100 gene stretches on the respective chromosomes, helping to identify malignant cells. (F,G) Pseudo-time trajectory analysis of epithelial cells from normal lung, primary tumor (green), and brain metastasis (red) samples shows the expression levels of *ANKRD11* decrease as the tumor progresses and metastasizes, with the black line representing the smoothed expression trend of *ANKRD11*. ① and ② indicate branch points along the pseudotime trajectory. BM, brain metastasis; PT, primary tumor; CNV, copy number variation; UMAP, Uniform Manifold Approximation and Projection.

from the datasets for more detailed analysis. Uniform Manifold Approximation and Projection (UMAP) plots of these epithelial cells, colored according to their tissue of origin, demonstrated distinct clustering patterns for cells from normal lung, primary tumors, and BMs (*Figure 3C*), and showed the differences in *ANKRD11* expression among clusters (*Figure 3D*). Besides, we evaluated large-scale CNVs in these epithelial cells. Hierarchical heatmaps of CNVs revealed gains and losses across various chromosomes, helping to distinguish malignant cells from normal ones (*Figure 3E*). Subsequently, we characterized the expression of *ANKRD11* along the pseudo-time trajectory in these epithelial cells. Our results showed that *ANKRD11* expression decreased progressively from normal lung tissue to primary tumors and further to BMs (*Figure 3F,3G*), which suggested that reduced *ANKRD11* expression correlated with LUAD progression and metastasis.

ANKRD11 suppresses tumor invasion and metastasis via upregulating KRT6A

ANKRD11 knockdown assays were then performed in A549 and PC9 LUAD cell lines to validate its functional impact on tumor cells. Transwell migration assays revealed that *ANKRD11* knockdown significantly enhanced the invasive capability of these cells (P<0.01 for both cell lines) (*Figure 4A,4B*). Additionally, scratch wound healing assays demonstrated that *ANKRD11* knockdown increased the migration ability of A549 and PC9 cells (*Figure 4C*).

Then, to explore the molecular mechanisms underlying these phenotypic changes and further identify potential downstream targets of *ANKRD11*, bulk RNA sequencing was performed on *ANKRD11* knockdown cell lines and their control cell lines. The differential gene expression analysis revealed significant changes in gene expression profiles between the knockdown and control groups, as illustrated by the heatmap (*Figure 4D*) and volcano plot (*Figure 4E*). Notably, *KRT6A* emerged as the most significantly upregulated gene in the *ANKRD11* knockdown cells, suggesting its potential role as a downstream effector of *ANKRD11* in promoting lung cancer cell migration. Kaplan-Meier survival analysis of LUAD patients, using data from public databases, confirmed that higher *KRT6A* expression was associated with poorer OS (logrank P<0.001) (*Figure 4F*). Single-cell expression analysis using pseudo-time trajectory mapping of *KRT6A* expression in epithelial cells from normal lung, primary tumors, and BMs revealed a clear increasing trend of *KRT6A* expression along the progression from normal tissue to BM (*Figure 4G,4H*).

To investigate the role of *KRT6A* in BM, we performed a series of *in vitro* experiments, demonstrating that *KRT6A* knockdown significantly reduced the migration ability of tumor cells compared to the negative control (*Figure 5A-5C*). To further explore the functional interaction between *KRT6A* and *ANKRD11*, we conducted cross-rescue experiments. The results revealed that *KRT6A* knockdown in *ANKRD11*-knockdown cells partially suppressed the enhanced migratory phenotype induced by *ANKRD11* silencing (*Figure 5D,5E*). These findings suggest a functional interplay between *KRT6A* and *ANKRD11* in regulating tumor cell migration. In addition, Western blot analysis indicated that *ANKRD11* knockdown led to an upregulation of *KRT6A* expression, along with that in metastasis-related markers *SNAI1* (21) (*Figure 5F*). Collectively, these results highlight the pivotal role of *KRT6A* in mediating tumor cell migration and its functional connection with *ANKRD11* in the metastatic process.

ANKRD11 knockdown promotes brain metastatic progression in nude mice model

To evaluate the role of *ANKRD11* in BM, we conducted *in vivo* experiments using a 3v3 nude mice model. Fluorescence imaging revealed that mice in the *ANKRD11* knockdown group exhibited significantly stronger metastatic signals compared to the control group, suggesting an enhanced metastatic burden in the brain (*Figure 6A*).

Histological analysis using HE staining confirmed the presence of metastatic foci in the brain tissues of the si*ANKRD11* group (*Figure 6B*), whereas no obvious metastatic lesions were observed in the control group (*Figure 6C*). Quantitative analysis, based on all 5 mice in each group, showed that the tumor weight in the BM sites was significantly higher in the si*ANKRD11* group compared to the control group (*Figure 6D*).

These results demonstrate that *ANKRD11* knockdown promotes tumor progression and increases the metastatic burden in the brain, underscoring its critical role in the metastatic cascade.

Discussion

LUAD is particularly prone to BM, which occurs in 20–40% of NSCLC patients and leads to significant morbidity and mortality (22), highlighting the urgent need for novel biomarkers to predict this process. The invasive nature of

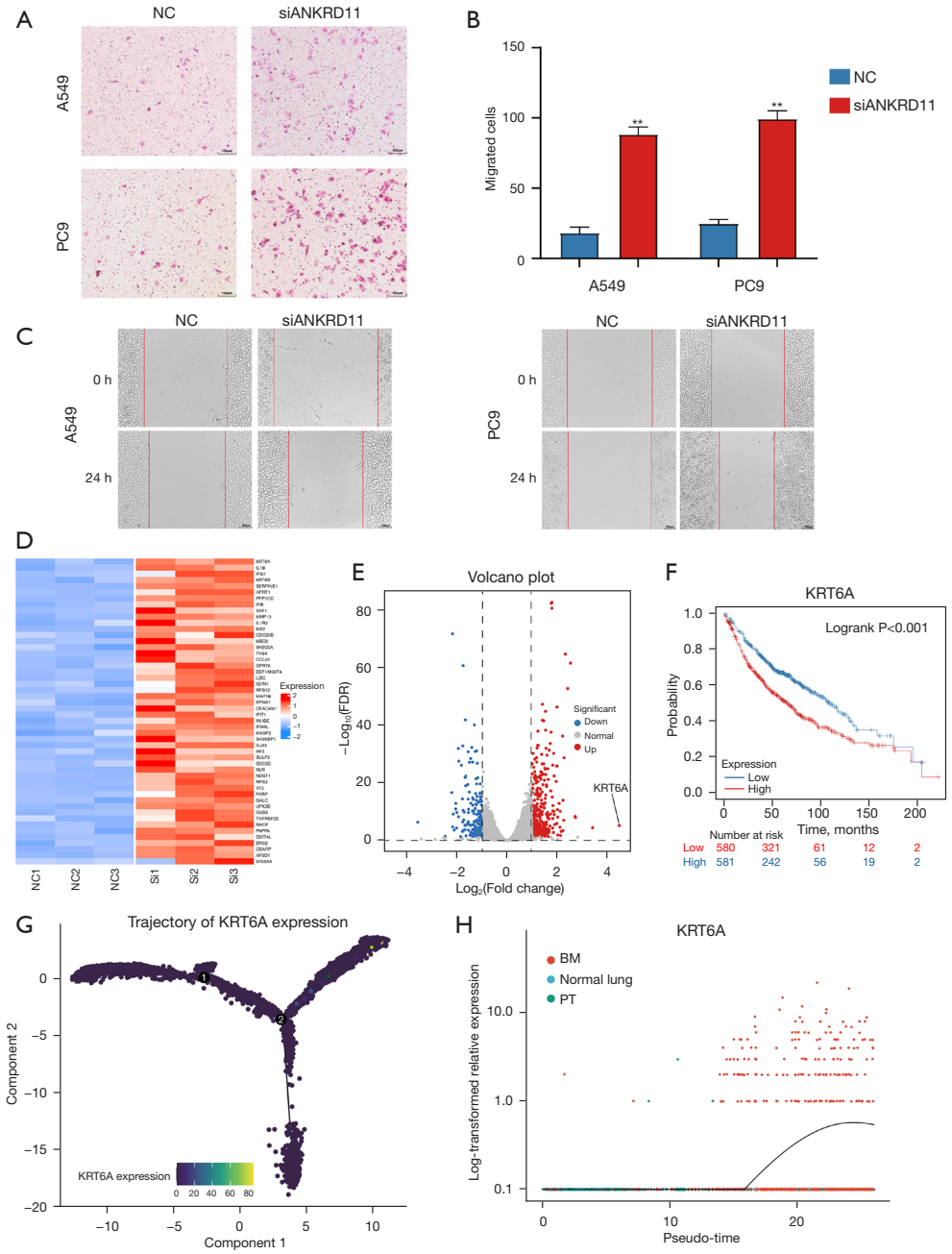

Figure 4 *ANKRD11* knockdown facilitates tumor cell migration and reveals *KRT6A* as a downstream target. (A,B) Transwell migration assay showing that *ANKRD11* knockdown significantly enhances the migration ability of A549 and PC9 lung adenocarcinoma (LUAD) cells compared to the negative control. Scale bar: 100 μm. Staining: crystal violet. (C) Scratch wound healing test indicating that *ANKRD11* knockdown enhances the migration ability of A549 and PC9 cells. (D) Heatmap of the top 50 most differentially expressed genes following *ANKRD11* knockdown in lung cancer cell lines. (E) Volcano plot of differential gene expression analysis from bulk RNA sequencing of *ANKRD11* knockdown cells. *KRT6A* was identified as the most significantly upregulated gene. (F) Kaplan-Meier survival analysis of lung adenocarcinoma patients stratified by *KRT6A* expression levels using a public database. Patients with higher *KRT6A* expression exhibited poorer overall survival. (G,H) Pseudotime trajectory analysis of *KRT6A* expression in epithelial cells shows an increase in *KRT6A* expression as the tumor progresses, with the black line representing the smoothed expression trend from normal lung tissue through primary tumor to BM. ① and ② indicate branch points along the pseudotime trajectory. **, P<0.01. BM, brain metastasis; PT, primary tumor; si*ANKRD11*, small interfering RNA targeting *ANKRD11*; NC, negative control; FDR, false discovery rate.

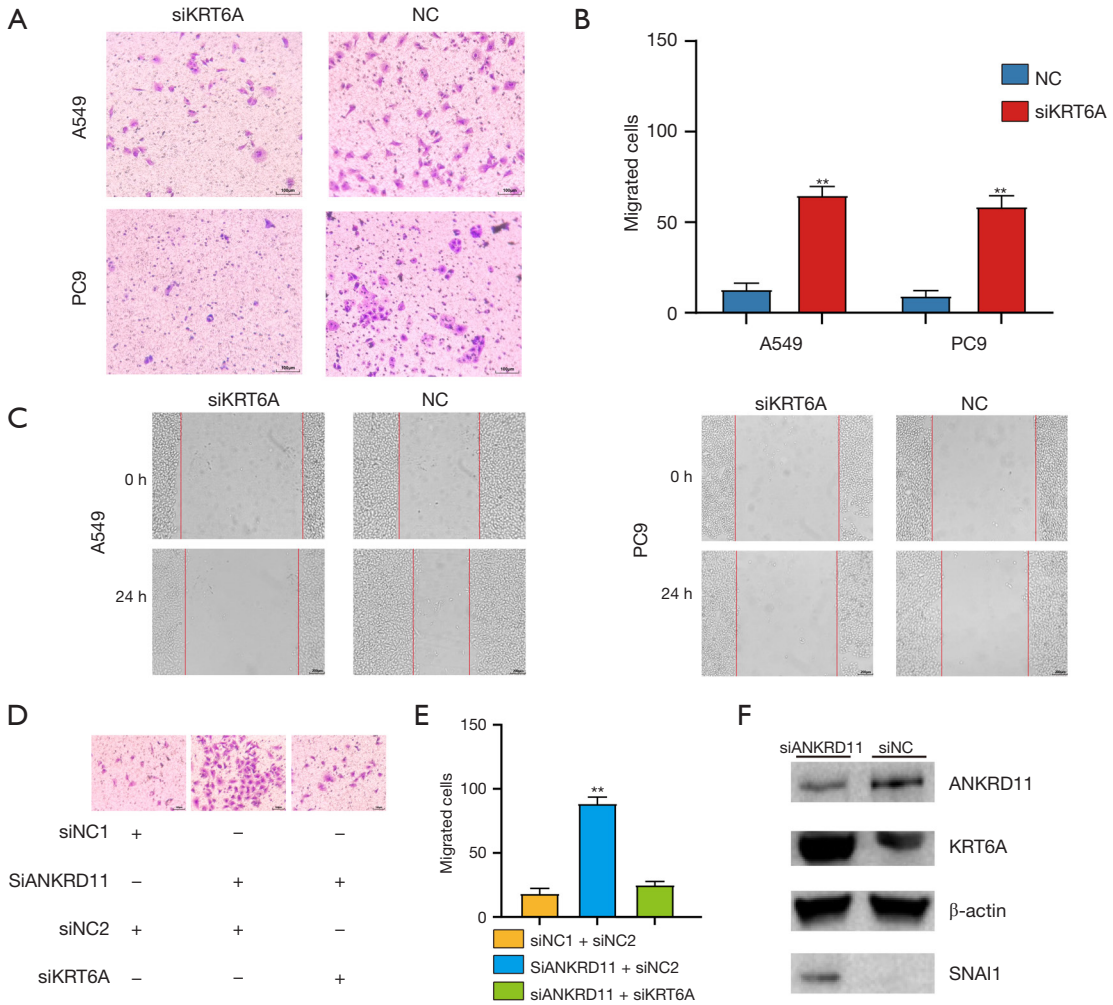

Figure 5 *KRT6A* knockdown attenuates tumor cell migration and demonstrates functional interaction with *ANKRD11*. (A,B) Transwell migration assay showing that *KRT6A* knockdown significantly reduces the migration ability of A549 and PC9 LUAD cells compared to the negative control. Scale bar: 100 μm. Staining: crystal violet. (C) Scratch wound healing test indicating that *KRT6A* knockdown reduces the migration ability of A549 and PC9 cells. (D,E) Transwell migration assay in cross-rescue experiments showing that *KRT6A* knockdown in *ANKRD11* knockdown cells partially suppressed the migratory phenotype. siNC1 and siNC2 represent negative control siRNAs. Scale bar: 100 μm. Staining: crystal violet. (F) Western blot result shows that *ANKRD11* knockdown increases the expression of *KRT6A* and the metastasis-related gene. **, P<0.01. si, small interfering; NC, negative control; LUAD, lung adenocarcinoma.

traditional tissue biopsies poses challenges in these cases. However, liquid biopsy, including the analysis of CSF, offers a less invasive alternative, providing critical insights into the genetic alterations associated with metastasis (23).

Our study demonstrates that CSF liquid biopsy is a powerful tool for identifying key mutational features in BM-LUAD. We detected high frequencies of mutations in genes such as *EGFR*, *BRCA2*, and *ANKRD11* despite the challenges posed by low ctDNA concentrations. The predominance of C > T and C > G Tis, linked to smoking, and an elevated Ti/Tv ratio indicating increased genomic instability, were correlated with the aggressive, metastatic nature of the disease in our patient cohort. Furthermore, we identified *ANKRD11* as a potential target gene and examined its differential expression in tumor versus normal tissues, as well as its impact on prognosis, using public datasets.

ScRNA-seq provided additional insights, revealing the cellular heterogeneity within normal lung tissue, primary lung tumors, and BMs. The identification of distinct cell

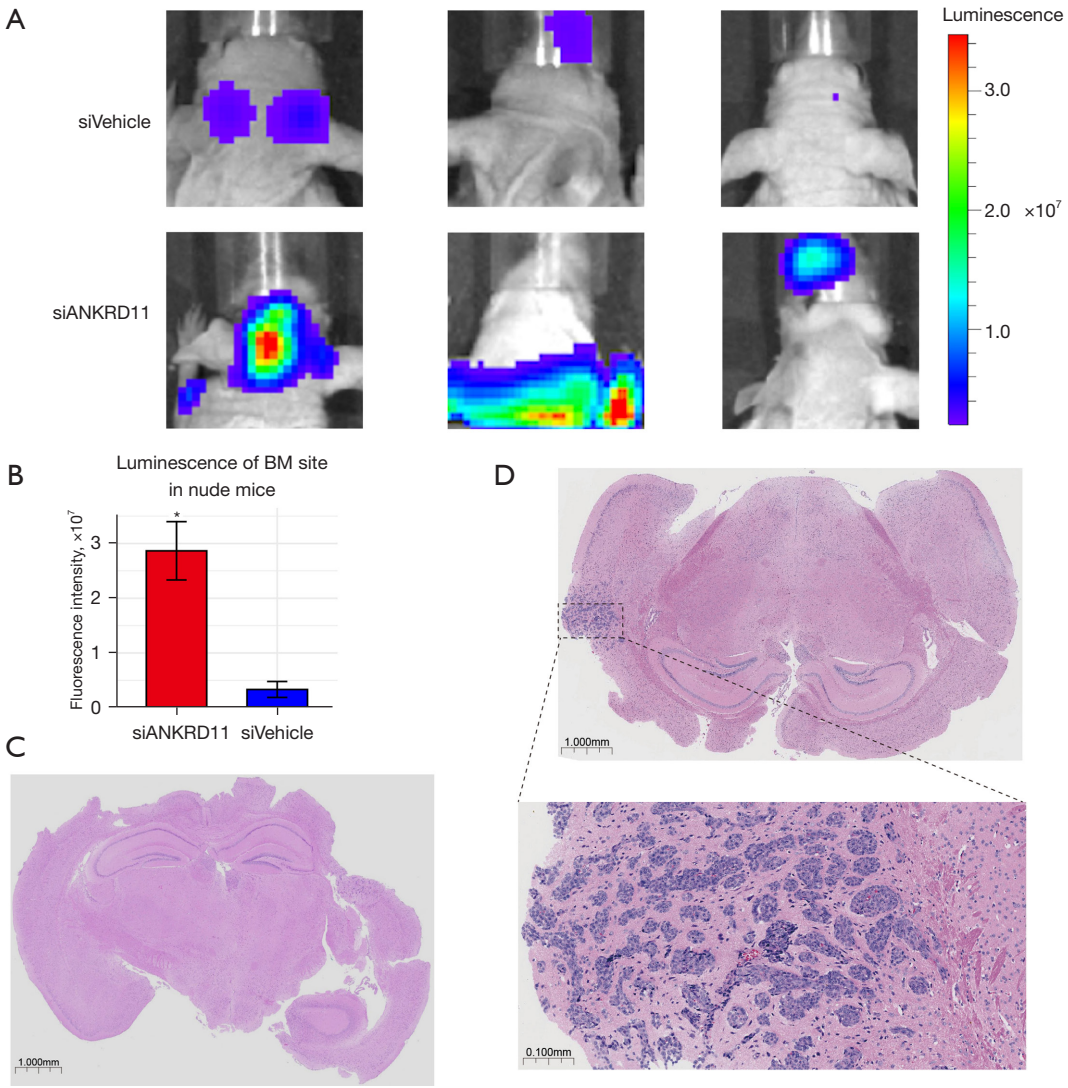

Figure 6 Validation of *ANKRD11* knockdown effects and *in vivo* analysis. (A) Fluorescence imaging of nude mice injected with lung adenocarcinoma cells shows increased brain metastasis signals in the *ANKRD11* knockdown group (si*ANKRD11*) compared to control. (B) The Luminescence of brain metastases tumor was significantly stronger in the si*ANKRD11* group than in the control group. (C) HE staining of the siNC control group revealed no obvious metastatic foci in the brain tissue. Scale bar: 1.000 mm. (D) HE staining results demonstrated the presence of metastatic foci in the brain of the si*ANKRD11* group. Scale bar: 1.000 and 0.100 mm. *, P<0.05. BM, brain metastasis; si*ANKRD11*, small interfering RNA targeting *ANKRD11*; siVehicle, small interfering RNA vehicle control; NC, negative control; HE, hematoxylin and eosin.

clusters and their subsequent annotation demonstrated the diverse cellular landscape and the progressive changes from normal epithelial cells to metastatic cells. The progressive decrease in *ANKRD11* expression from normal lung tissue to BMs, as shown by pseudotime trajectory analysis, suggests a close association between reduced *ANKRD11* expression and tumor progression. Such a trend stresses the potential role of *ANKRD11* as a tumor suppressor, where its downregulation may facilitate metastatic behavior in LUADs. The findings highlight the significance of *ANKRD11* in tumor progression, suggesting that its reduced expression may play a crucial role in facilitating metastasis. Furthermore, the detailed cellular and genomic landscape unveiled by this study underscores the importance

of integrating single-cell profiling with genomic analyses to fully understand the complexities of cancer metastasis. Single-cell analysis allows for the dissection of tumor heterogeneity, revealing the diverse cellular states and Tis that contribute to disease progression.

The *in vivo* and *in vitro* assays showed that *ANKRD11* downregulation enhanced tumor cell migration and invasion. *KRT6A* upregulation following *ANKRD11* knockdown, its association with poorer survival in LUAD patients, and its increased expression from normal tissue to metastasis implicate *KRT6A* in the metastatic process. Che *et al.* (2021) discovered that *KRT6A* promotes lung cancer cell growth and invasion through the *MYC*-regulated pentose phosphate pathway (24). Similarly, Xu *et al.* (2024) found that *KRT6A* enhances radioresistance, invasion, and metastasis in lung cancer via the p53 signaling pathway (25), while *ANKRD11* is a known coactivator of p53. Combined with our findings, these results suggest that *KRT6A* may play a pivotal role in mediating the effects of *ANKRD11* loss.

Our finding aligns with the established role of tumor suppressors in inhibiting cancer progression through various mechanisms. In the study by Neilsen *et al.*, *ANKRD11* functions as a coactivator of *p53*, enhancing its transcriptional activity and promoting the expression of *p53* target genes involved in cell cycle regulation and apoptosis. This interaction is essential for maintaining genomic stability and suppressing tumorigenesis (26). Similarly, Zhu *et al.* identified a high mutation rate of the *ANKRD11* gene in ovarian cancer, consistent with our findings. Mutations in *ANKRD11* have been shown to significantly reduce its protein expression by affecting protein stability, indicating that these loss-of-function mutations may contribute to cancer development. For instance, studies have identified *ANKRD11* as a potential susceptibility gene for ovarian cancer, where its mutations are associated with increased cancer risk and compromised tumor suppression (27). Furthermore, work by Yuan *et al.* and Kushner *et al.* has provided evidence that the loss of *ANKRD11* promotes the progression and aggressiveness of breast cancer by disrupting pathways involved in cell proliferation and metastasis (28,29). In breast cancer models, *ANKRD11* loss has been linked to increased epithelial-mesenchymal transition (EMT) and enhanced invasive potential, further supporting its role as a tumor suppressor. Collectively, these findings position *ANKRD11* as a critical gene for further investigation, not only in its mechanistic roles but also in its potential as a therapeutic target and biomarker across various cancer types.

There are several limitations in this study. The absence of control groups in our cohort posed a challenge, which was addressed by incorporating publicly available data. Additionally, the small sample size may reduce the statistical power and generalizability of our findings. To partially address this, we incorporated additional analyses using publicly available datasets, which provided supplementary evidence for *ANKRD11* as a biomarker for BM. These datasets complement the findings from our original cohort, enhancing the robustness of the study. Furthermore, the use of panel sequencing restricts the scope of our findings to a predefined set of genes. However, panel sequencing was chosen due to its practical advantages, including cost-effectiveness, higher sequencing depth, and clinical applicability, particularly for CSF samples where ctDNA levels are often very low. To mitigate this limitation, we validated our findings using independent public datasets, which consistently demonstrated enrichment of *ANKRD11* mutations in BM compared to non-brain metastatic cases. We also acknowledge that the lack of paired primary tumor tissues weakens the credibility of our findings. Therefore, we performed PCR validation of *ANKRD11* mutations in the primary tumor tissue of one patient, and the result confirmed the presence of the mutation, consistent with those detected in the CSF samples. Larger, prospective cohorts will be necessary in future research to further validate the clinical utility of *ANKRD11* and to explore its mechanistic roles in BM. Furthermore, due to the transient nature of siRNA knockdown, maintaining stable gene suppression over an extended period was not feasible, which restricted the inclusion of immunohistochemistry (IHC) data. To address this limitation, we have instead incorporated HE-stained histological analyses of BMs, including both the experimental and control groups, to provide a clearer visualization of tumor burden. Functional studies should aim to delineate the interactions between *ANKRD11* alteration and other key molecular events involved in metastasis, potentially uncovering new therapeutic targets.

Our study demonstrates the potential of CSF liquid biopsy to identify novel biomarkers for BM-LUAD, and the results identified *ANKRD11* as a predictive biomarker for BM-LUAD.

Conclusions

Our study demonstrates the potential of CSF liquid biopsy to identify novel biomarkers for BM-LUAD through *in vitro*

and *in vivo* validation, and we identified that *ANKRD11* as a predictive biomarker for BM-LUAD. These findings address, to some extent, the existing gap in biomarkers for BM-LUAD.

Acknowledgments

None.

Footnote

Reporting Checklist: The authors have completed the ARRIVE and MDAR reporting checklists. Available at https://tlcr.amegroups.com/article/view/10.21037/tlcr-24-800/rc

Data Sharing Statement: Available at https://tlcr.amegroups.com/article/view/10.21037/tlcr-24-800/dss

Peer Review File: Available at https://tlcr.amegroups.com/article/view/10.21037/tlcr-24-800/prf

Funding: This study was supported by the grant from National Natural Science Foundation of China (Nos. 82203202 and 82472724).

Conflicts of Interest: All authors have completed the ICMJE uniform disclosure form (available at https://tlcr.amegroups.com/article/view/10.21037/tlcr-24-800/coif). The authors have no conflicts of interest to declare.

Ethical Statement: The authors are accountable for all aspects of the work in ensuring that questions related to the accuracy or integrity of any part of the work are appropriately investigated and resolved. The study was conducted in accordance with the Declaration of Helsinki (as revised in 2013) and was approved by the Ethics Committee of the Jing County Hospital (No. 2020-007). Written informed consent was obtained from all patients included in the study. All animal experiments were conducted under a project license (No. IACUC2404078) approved by the Institutional Animal Care and Use Committee (IACUC) of Nanjing Medical University, in compliance with the national and institutional guidelines for the care and use of laboratory animals.

References

1. Denisenko TV, Budkevich IN, Zhivotovsky B. Cell death-based treatment of lung adenocarcinoma. Cell Death Dis 2018;9:117.
2. Siegel RL, Miller KD, Wagle NS, et al. Cancer statistics, 2023. CA Cancer J Clin 2023;73:17-48.
3. Preusser M, Capper D, Ilhan-Mutlu A, et al. Brain metastases: pathobiology and emerging targeted therapies. Acta Neuropathol 2012;123:205-22.
4. Riihimäki M, Hemminki A, Fallah M, et al. Metastatic sites and survival in lung cancer. Lung Cancer 2014;86:78-84.
5. Alix-Panabières C, Pantel K. Liquid Biopsy: From Discovery to Clinical Application. Cancer Discov 2021;11:858-73.
6. Pantel K, Alix-Panabières C. Liquid biopsy and minimal residual disease - latest advances and implications for cure. Nat Rev Clin Oncol 2019;16:409-24.
7. Rehman AU, Khan P, Maurya SK, et al. Liquid biopsies to occult brain metastasis. Mol Cancer 2022;21:113.
8. Eibl RH, Schneemann M. Liquid Biopsy and Primary Brain Tumors. Cancers (Basel) 2021;13:5429.
9. Li YS, Zheng MM, Jiang BY, et al. Association of Cerebrospinal Fluid Tumor DNA Genotyping With Survival Among Patients With Lung Adenocarcinoma and Central Nervous System Metastases. JAMA Netw Open 2020;3:e209077.
10. Kim N, Kim HK, Lee K, et al. Single-cell RNA sequencing demonstrates the molecular and cellular reprogramming of metastatic lung adenocarcinoma. Nat Commun 2020;11:2285.
11. Patel AP, Tirosh I, Trombetta JJ, et al. Single-cell RNA-seq highlights intratumoral heterogeneity in primary glioblastoma. Science 2014;344:1396-401.
12. Satija R, Farrell JA, Gennert D, et al. Spatial reconstruction of single-cell gene expression data. Nat Biotechnol 2015;33:495-502.
13. Qiu X, Mao Q, Tang Y, et al. Reversed graph embedding resolves complex single-cell trajectories. Nat Methods

2017;14:979-82.
14. Győrffy B. Transcriptome-level discovery of survival-associated biomarkers and therapy targets in non-small-cell lung cancer. Br J Pharmacol 2024;181:362-74.
15. Győrffy B. Integrated analysis of public datasets for the discovery and validation of survival-associated genes in solid tumors. Innovation (Camb) 2024;5:100625.
16. Wan JCM, Massie C, Garcia-Corbacho J, et al. Liquid biopsies come of age: towards implementation of circulating tumour DNA. Nat Rev Cancer 2017;17:223-38.
17. Alexandrov LB, Nik-Zainal S, Wedge DC, et al. Signatures of mutational processes in human cancer. Nature 2013;500:415-21.
18. Nguyen DX, Bos PD, Massagué J. Metastasis: from dissemination to organ-specific colonization. Nat Rev Cancer 2009;9:274-84.
19. Jordan EJ, Kim HR, Arcila ME, Barron D, Chakravarty D, Gao J, et al. Prospective Comprehensive Molecular Characterization of Lung Adenocarcinomas for Efficient Patient Matching to Approved and Emerging Therapies. Cancer Discov 2017;7:596-609.
20. Skakodub A, Walch H, Tringale KR, Eichholz J, Imber BS, Vasudevan HN, et al. Genomic analysis and clinical correlations of non-small cell lung cancer brain metastasis. Nat Commun 2023;14:4980.
21. Wang X, Liu R, Zhu W, et al. UDP-glucose accelerates SNAI1 mRNA decay and impairs lung cancer metastasis. Nature 2019;571:127-31.
22. Zhu Y, Cui Y, Zheng X, et al. Small-cell lung cancer brain metastasis: From molecular mechanisms to diagnosis and treatment. Biochim Biophys Acta Mol Basis Dis 2022;1868:166557.
23. Li W, Liu JB, Hou LK, et al. Liquid biopsy in lung cancer: significance in diagnostics, prediction, and treatment monitoring. Mol Cancer 2022;21:25.
24. Che D, Wang M, Sun J, et al. KRT6A Promotes Lung Cancer Cell Growth and Invasion Through MYC-Regulated Pentose Phosphate Pathway. Front Cell Dev Biol 2021;9:694071.
25. Xu Q, Yu Z, Mei Q, et al. Keratin 6A (KRT6A) promotes radioresistance, invasion, and metastasis in lung cancer via p53 signaling pathway. Aging (Albany NY) 2024;16:7060-72.
26. Neilsen PM, Cheney KM, Li CW, et al. Identification of ANKRD11 as a p53 coactivator. J Cell Sci 2008;121:3541-52.
27. Zhu Q, Zhang J, Chen Y, et al. Whole-exome sequencing of ovarian cancer families uncovers putative predisposition genes. Int J Cancer 2020;146:2147-55.
28. Yuan M, Barefoot ME, Peterson K, et al. Loss of ANCO1 Expression Regulates Chromatin Accessibility and Drives Progression of Early-Stage Triple-Negative Breast Cancer. Int J Mol Sci 2023;24:11505.
29. Kushner MH, Ory V, Graham GT, et al. Loss of ANCO1 repression at AIB1/YAP targets drives breast cancer progression. EMBO Rep 2020;21:e48741.

Cite this article as: Sun Q, Xing P, Wang Q, Xia Z, Li J, Li Z, Meng F, Liu T, Wang S, Yin R. *ANKRD11* as a potential biomarker for brain metastasis from lung adenocarcinoma via cerebrospinal fluid liquid biopsy. Transl Lung Cancer Res 2025;14(3):662-676. doi: 10.21037/tlcr-24-800